Self-Assembled All-Conjugated Block Copolymer as an Effective Hole Conductor for Solid-State Dye-Sensitized Solar Cells

Wei-Chih Chen,[†] Yi-Huan Lee,[†,‡] Chia-Yuan Chen,[§] Kuo-Chang Kau,[‡] Lu-Yin Lin,[‡] Chi-An Dai,[†,‡,*] Chun-Guey Wu,[§,*] Kuo-Chuan Ho,[†,‡] Juen-Kai Wang,[⊥] and Leeyih Wang[†,⊥,*]

[†]Institute of Polymer Science and Engineering and [‡]Department of Chemical Engineering, National Taiwan University, Taipei, 10617 Taiwan, ROC, [§]Department of Chemistry, National Central University, Jung-Li, 32001 Taiwan, ROC, and [⊥]Center for Condensed Matter Sciences, National Taiwan University, Taipei, 10617 Taiwan, ROC

ABSTRACT An all-conjugated diblock copolymer, poly(2,5-dihexyloxy-*p*-phenylene)-*b*-poly(3-hexylthiophene) (PPP-*b*-P3HT), was synthesized and applied as a hole transport material (HTM) for the fabrication of solid-state dye-sensitized solar cells (ss-DSCs). This copolymer is characterized by an enhanced crystallinity, enabling its P3HT component to self-organize into interpenetrated and long-range-ordered crystalline fibrils upon spin-drying and ultimately endowing itself to have a faster hole mobility than that of the parent P3HT homopolymer. Transient photovoltage measurements indicate that the photovoltaic cell based on PPP-*b*-P3HT as the HTM has a longer electron lifetime than that of the reference device based on P3HT homopolymer. Moreover, comparing the two ss-DSCs in terms of the electrochemical impedance spectra reveals that the electron density in the TiO_2 conduction band is substantially higher in the PPP-*b*-P3HT device than in the P3HT cell. Above observations suggest that the PPP block facilitates an intimate contact between the copolymer and dye molecules absorbed on the nanoporous TiO_2 layer, which significantly enhances the performance of the resulting device. Consequently, the PPP-*b*-P3HT ss-DSC exhibits a promising power conversion efficiency of 4.65%. This study demonstrates that conjugated block copolymers can function as superior HTMs of highly efficient ss-DSCs.

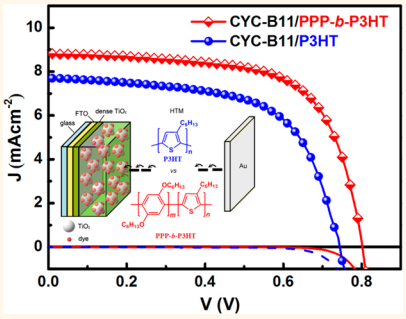

KEYWORDS: block copolymer · conjugated polymers · hole transport materials · self-assembly · solid-state dye-sensitized solar cells

By taking advantage of a simple device fabrication process, inexpensive manufacturing equipment, and broad selection of low-cost materials, dye-sensitized solar cells (DSCs) have been considered as a promising candidate for the next-generation energy source.[1,2] In particular, their power conversion efficiency (PCE) has recently reached 12% after successive advances in sensitizers and electrolytes.[3] However, the application of conventional DSCs often suffers from inadequate device stability and possible environmental pollution resulting from the potential leakage of liquid electrolytes upon long-term operation.[4] Quasi- and all- solid-state DSCs (ss-DSCs) have thus aroused considerable attention in the past decade;[5−7] meanwhile, various organic and inorganic compounds were designed and applied successfully as a hole transport material (HTM).[8−10] Among them, 2,2′,7,7′-tetrakis-(*N*,*N*-di-*p*-methoxyphenylamine)-9,9′-spirobifluorene (OMeTAD) is the most popular material, owing to its adequate hole mobility and amorphous characteristic.[11] Another class of promising HTMs is organic conjugated polymers, which typically possess a superior film-formation property that promotes the construction of smooth and continuous pathways inside the mesopores of the TiO_2 layer for transporting holes to the cathode,[12] as well as strong absorption of visible and even near-infrared light that can principally enhance the light-harvesting capacity of the cell and thus contribute to the photocurrent *via* charge and/or energy transfer routes.[13−16] To achieve high-performance ss-DSCs, the carrier mobility and the pore-filling ability of solid-state HTMs are identified as two decisive factors.[12,17−20]

* Address correspondence to leewang@ntu.edu.tw (L.W.), t610002@cc.ncu.edu.tw (C.-G.W.), polymer@ntu.edu.tw (C.-A.D.).

Received for review August 20, 2013 and accepted January 20, 2014.

Published online January 20, 2014
10.1021/nn404346v

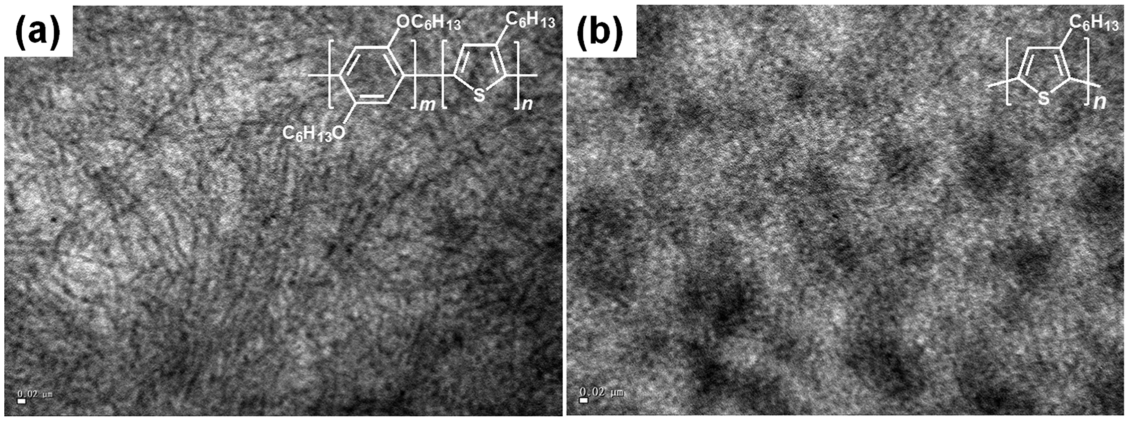

Figure 1. TEM images of the spin-coated solid films of (a) PPP-*b*-P3HT and (b) P3HT. Inset: chemical structure of PPP-*b*-P3HT and P3HT.

Moreover, a high structural compatibility between the sensitizer and the HTM improves the efficiency of dye regeneration, leading to an increase in the PCE.[21]

As an interesting and important class of functional material, diblock copolymer can self-organize into a variety of highly ordered structures with characteristic lengths ranging from nanometers to micrometers. Moreover, different phase morphologies can be achieved by varying the chain length and/or the composition of the two blocks.[22,23] Recent literature has indicated that poly(2,5-dihexyloxy-*p*-phenylene)-*b*-poly(3-hexylthiophene) (PPP-*b*-P3HT), an all-conjugated block copolymer, features a good self-assembly ability and crystallinity,[24] rendering its potential application in optoelectronics. However, to our knowledge, the feasibility of using block copolymers as the HTMs of ss-DSCs has not yet been established successfully. This study demonstrates that PPP segments in the copolymer improve the molecular packing of the P3HT blocks to form interpenetrated and long-range-ordered fibrils during spin-drying, leading to a faster hole mobility for the block copolymer than that of the parent P3HT homopolymer with a comparable molecular weight. More importantly, as this diblock copolymer is applied as the HTM of ss-DSCs, the PPP chain significantly improves both the completeness and tightness of the HTM coverage on top of the sensitized titania such that the probability of carrier recombination is lowered, leading to a significant advance in photovoltaic performance.

RESULTS AND DISCUSSION

As depicted in Scheme S1 (see Supporting Information), the PPP-*b*-P3HT block copolymer was synthesized by using Grignard metathesis (GRIM) polymerization of 2,5-dibromo-3-hexylthiophene from an end-living PPP block, which was first prepared by using Ni(dppe)Cl_2-catalyzed cross-coupling of 4-bromo-2,5-bis(hexyloxy)phenylmagnesium bromide monomer, where dppe stands for 1,2-bis(diphenylphoshino)-ethane as a ligand for the Ni catalyst. Both PPP homopolymer and PPP-*b*-P3HT yield monomodal gel permeation chromatography (GPC) traces (Figure S1) with polydispersity indices (PDI) of 1.29 and 1.32, respectively, suggesting a complete capping of PPP block with P3HT chain to produce a well-defined copolymer. By using a set of polystyrene samples as standard, the number-average molecular weights (M_n) of PPP and P3HT were determined to be 8000 and 27000 g/mol, respectively, which are equivalent to a degree of polymerization of 29 for the PPP and 163 for the P3HT segments. Furthermore, the ^{1}H NMR spectrum (Figure S2) reveals that the P3HT block in the copolymer has a head-to-tail regioregularity of ~93%. For comparison, a P3HT homopolymer with an M_n of 33000 g/mol and a regioregularity of ~93% was also prepared by the Grignard metathesis method. The chemical structures of the PPP-*b*-P3HT block copolymer and the corresponding P3HT homopolymer are presented in the inset of Figure 1.

Yu *et al.* demonstrated that the PPP-*b*-P3HT copolymer can self-assemble into crystalline fibrils by modulating the competition between the crystallization of the conjugated backbone and the microphase separation of the two blocks because of their thermodynamic incompatibility.[24] Figure 1 shows the transmission electron microscopy (TEM) micrographs of the PPP-*b*-P3HT and P3HT that were prepared as spin-coated thin films from their chlorobenzene solutions. Numerous dark-colored fibrils with lengths of several micrometers are observed in the film of PPP-*b*-P3HT, whereas the P3HT film has a rather disordered nodule-like structure, which is, nevertheless, still capable of self-assembling into crystallites during the spin-drying process,[25,26] indicating that the PPP-*b*-P3HT possesses higher crystallinity than the P3HT homopolymer. To identify the blocks in which the copolymer is associated with the formation of the fibrils, wide-angle X-ray scattering (WAXS) measurements were made on solid films of the PPP, P3HT homopolymers, and the PPP-*b*-P3HT. The WAXS spectra in Figure 2a show that the PPP homopolymer has a prominent diffraction peak at a scattering vector (q_z) of 0.300 Å^{-1}, corresponding to a

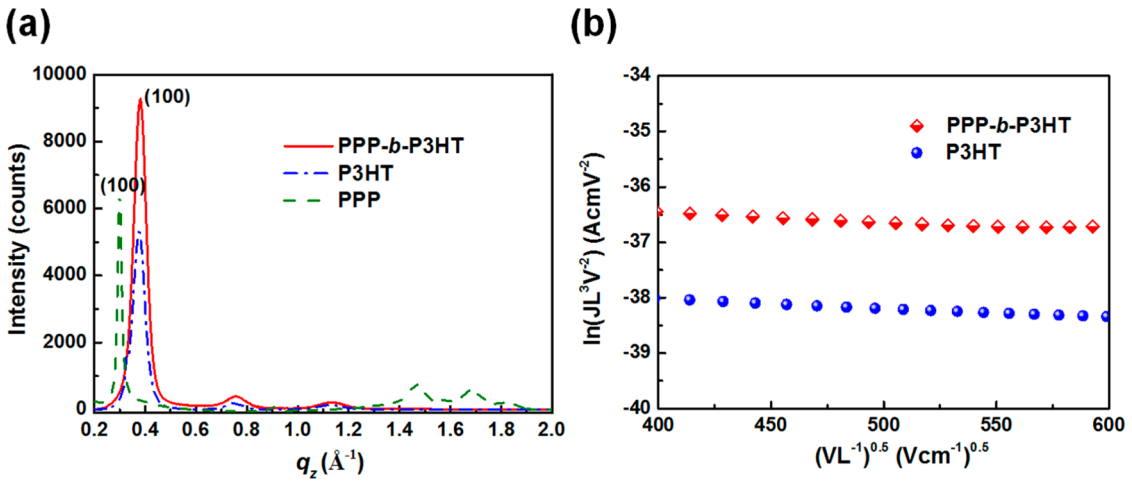

Figure 2. (a) WAXS spectra of PPP-*b*-P3HT, P3HT, and PPP solid films. (b) Plots of $\ln(JL^3/V^2)$ *vs* $(V/L)^{0.5}$ for the hole-only devices with a configuration of ITO/PEDOT:PSS/(PPP-*b*-P3HT or P3HT)/Au.

d-spacing of 2.09 nm, which is close to the value for the (100) plane of PPP reported previously in the literature.[24] However, the PPP-*b*-P3HT exhibits a diffraction spectrum similar to that obtained from the P3HT homopolymer with q_z values of 0.381, 0.758, and 1.134 Å^{-1}, corresponding to *d*-spacings of 1.65, 0.83, and 0.55 nm for the (100), (200), and (300) planes, respectively, of pristine crystalline P3HT lamellae. Notably, no diffraction peak in the spectra was associated with PPP for the copolymer. These observations clearly verify that the P3HT segments in the block copolymer tend to form a crystalline supramolecular structure through $\pi-\pi$ stacking of the P3HT during the spin-drying process while the PPP block remains as an amorphous structure. Furthermore, surprisingly, the introduction of a short PPP segment to form a block copolymer markedly facilitates the crystallization of the P3HT block, as indicated by the higher absolute diffraction intensity for the PPP-P3HT than for the P3HT on the same weight basis, as shown in Figure 2a.

When conjugated polymers are used in the field of optoelectronics, such as field-effect transistors and solar cells, their carrier mobility frequently dominates device performance. The hole mobilities of the P3HT and PPP-*b*-P3HT were evaluated in a hole-only diode configuration, ITO/PEDOT:PSS/(PPP-*b*-P3HT or P3HT)/Au, using the space-charge-limited current (SCLC) method.[27,28] Figure 2b plots the current density (*J*) against the applied voltage (*V*) as $\ln(JL^3/V^2)$ *versus* $(V/L)^{0.5}$, where *L* represents the thickness of the examined polymer film that is sandwiched between a PEDOT:PSS layer and a gold electrode. The zero-field hole mobility (μ_{h0}) can then be calculated from the intercept using the equation for the current density in the SCLC regime

$$J = \frac{9}{8}\varepsilon_r\varepsilon_0\mu_{h0}\frac{V^2}{L^3}\exp(0.89\sqrt{\frac{V}{E_0L}})$$

where ε_r is the dielectric constant of the sample, ε_0 is the permittivity of free space, and E_0 is the characteristic electric field. The value of μ_{h0} is 8.5×10^{-4} cm^2/Vs (E_0 = 3.8×10^5 V/cm) for the PPP-*b*-P3HT block copolymer and 1.9×10^{-4} cm^2/Vs (E_0 = 3.1×10^5 V/cm) for the P3HT homopolymer, revealing that the formation of a highly ordered and long-ranged fibrillar structure enhances the carrier mobility of polymeric materials and that the existence of PPP segments does not apparently disturb the transport of holes throughout the polymer film.

The methods of cyclic voltammetry (CV) and UV−vis spectrometry were combined to determine the energy levels of the two polymers. The energy of the highest occupied molecular orbital (HOMO) of the polymers was first obtained from the onset oxidation potential ($E_{ox,onset}$) of the cyclic voltammograms shown in Figure S3a using the formula of HOMO = $-[(E_{ox,onset} - E_{Fc+}) + 4.8$ eV], where E_{Fc+} denotes the measured oxidation potential of ferrocene and the 4.8 eV is the absolute oxidation potential value of ferrocence *in vacuo*. The HOMO energies for the PPP, P3HT homopolymers, and the PPP-*b*-P3HT are determined to be −4.98, −5.04, and −5.02 eV, respectively. The small band offset between the HOMO levels of the PPP and P3HT segments allows for an easy hopping of holes between the two blocks of the copolymer. This finding supports the high hole mobility of the PPP-*b*-P3HT, which was discussed earlier. The energies of the lowest unoccupied molecular orbital (LUMO) could then be estimated from the sum of the measured HOMO energies and the optical band gaps, which were determined from the wavelengths of the onset of absorption obtained from the corresponding UV−vis spectra in Figure S3b. Table 1 lists these experimental results. Both polymers have comparable LUMO energies of ∼−3.1 eV.

To compare the effectiveness of PPP-*b*-P3HT and P3HT as hole transport materials in ss-DSCs, photovoltaic devices with a structure of FTO/compact TiO_2/porous TiO_2:CYC-B11:HTM (PPP-*b*-P3HT or P3HT)/Au were fabricated. The sensitizer dye used for this study

TABLE 1. Fundamental Properties of PPP-*b*-P3HT and P3HT[a]

polymer	M_n (Da)	crystallite size (nm)	hole mobility (μ_{h0}, cm^2/Vs)	λ_{onset} (nm)	E_{0-0} (eV)	HOMO/LUMO (eV)
PPP	8000			381	3.25	−4.98/−1.73
PPP-*b*-P3HT	35000	8.1	8.5×10^{-4}	645	1.92	−5.02/−3.10
P3HT	33000	7.6	1.9×10^{-4}	645	1.92	−5.04/−3.12

[a] M_n, number-average molecular weight; λ_{onset}, onset wavelength of absorption spectrum; E_{0-0}, lowest transition energy.

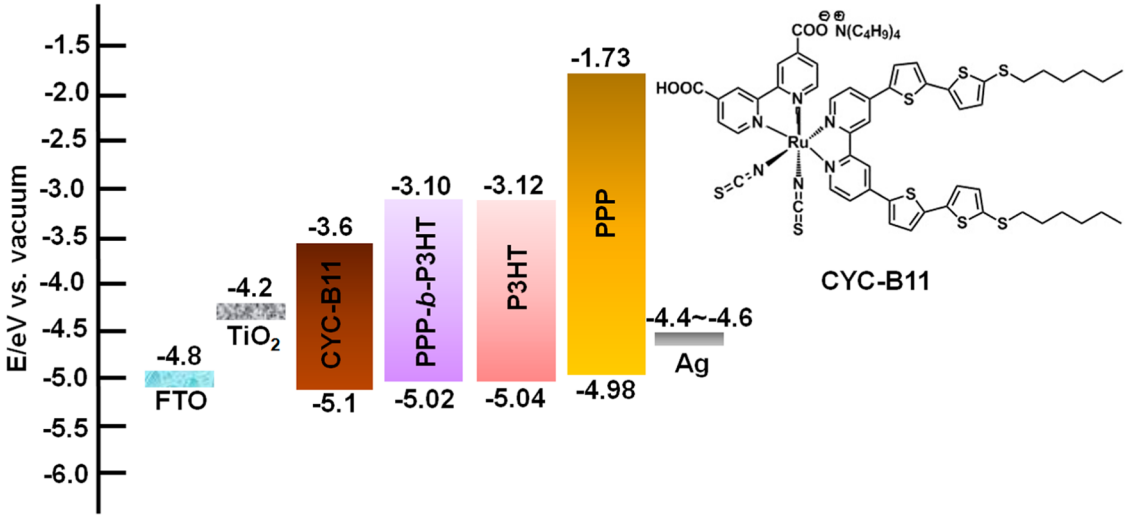

Figure 3. Schematic energy levels of the components in the ss-DSCs and the molecular structure of CYC-B11 dye.

is denoted as CYC-B11, whose chemical structure is displayed in Figure 3, which also depicts the energy levels of the components in the ss-DSCs. Both PPP-*b*-P3HT and P3HT have a higher-lying HOMO level than CYC-B11 does, suggesting that the regeneration of the oxidized dye molecules by these two polymers is energetically feasible. Moreover, their LUMO levels are above that of CYC-B11 and the conduction band of TiO_2, implying that the photoexcited electrons that are created in the HTMs can be smoothly transferred to TiO_2 and then contribute to the photocurrent.[29]

To have better understanding on the penetration efficiency of HTMs into the porous TiO_2 layer, the P3HT and PPP-*b*-P3HT were deposited onto the surface of a compact TiO_2 and a porous TiO_2 substrate using the same spin-coating process. A significantly thinner (~60 nm) polymer overlayer on the porous TiO_2 than that (~120 nm) on the compact TiO_2 was observed for both systems, as shown Figure S4, suggesting that these macromolecules effectively infiltrate the porous TiO_2 film during the drying procedure. Furthermore, the compact TiO_2 substrates are capped with P3HT and PPP-*b*-P3HT films of similar thickness that implies both polymer solutions have comparable viscosity. Similarly, thick overlayers of these two polymers on top of the porous TiO_2 are also obtained. These findings demonstrate that both systems exhibit comparable pore-filling fractions.

Figure 4a plots the dependence of the current density (J) on the applied bias (V) in the dark and under simulated AM 1.5G solar irradiation at 100 mW/cm^2. Table 2 presents photovoltaic parameters of the best cells, and the corresponding statistical data from seven devices are included in Table S1. Notably, replacing P3HT with PPP-*b*-P3HT as the HTM simultaneously increases the short-circuit current density (J_{sc}) and the open-circuit voltage (V_{oc}), thereby improving the device performance by more than 30%. The best CYC-B11/PPP-*b*-P3HT device herein exhibits a V_{oc} of 0.81 V, a J_{sc} of 8.81 mA/cm^2, and a FF of 65.2% and therefore an outstanding PCE of 4.65%. A simple method for estimating the series resistance (R_s) of a solar device is to find the reciprocal of the slope of its $J-V$ curve at V_{oc}. As shown in Table 2, the R_s of the CYC-B11/PPP-*b*-P3HT device is lower than that of the CYC-B11/P3HT device, consistent with the fact that the hole mobility of PPP-*b*-P3HT is approximately 4 times faster than that of the P3HT homopolymer. Rapid transportation of holes and electrons along the pathways that are established by the HTM and TiO_2, respectively, to the corresponding electrodes, suppresses the recombination of free carriers. Once the photogenerated excitons are dissociated into electrons and holes at the TiO_2/dye/HTM interface, the two charge carriers can be rapidly collected by the respective electrodes in the course of transportation without significant recombination losses, resulting in a high photocurrent for the copolymer device.

Although the CYC-B11/PPP-*b*-P3HT and CYC-B11/P3HT devices exhibit similar energy offsets between

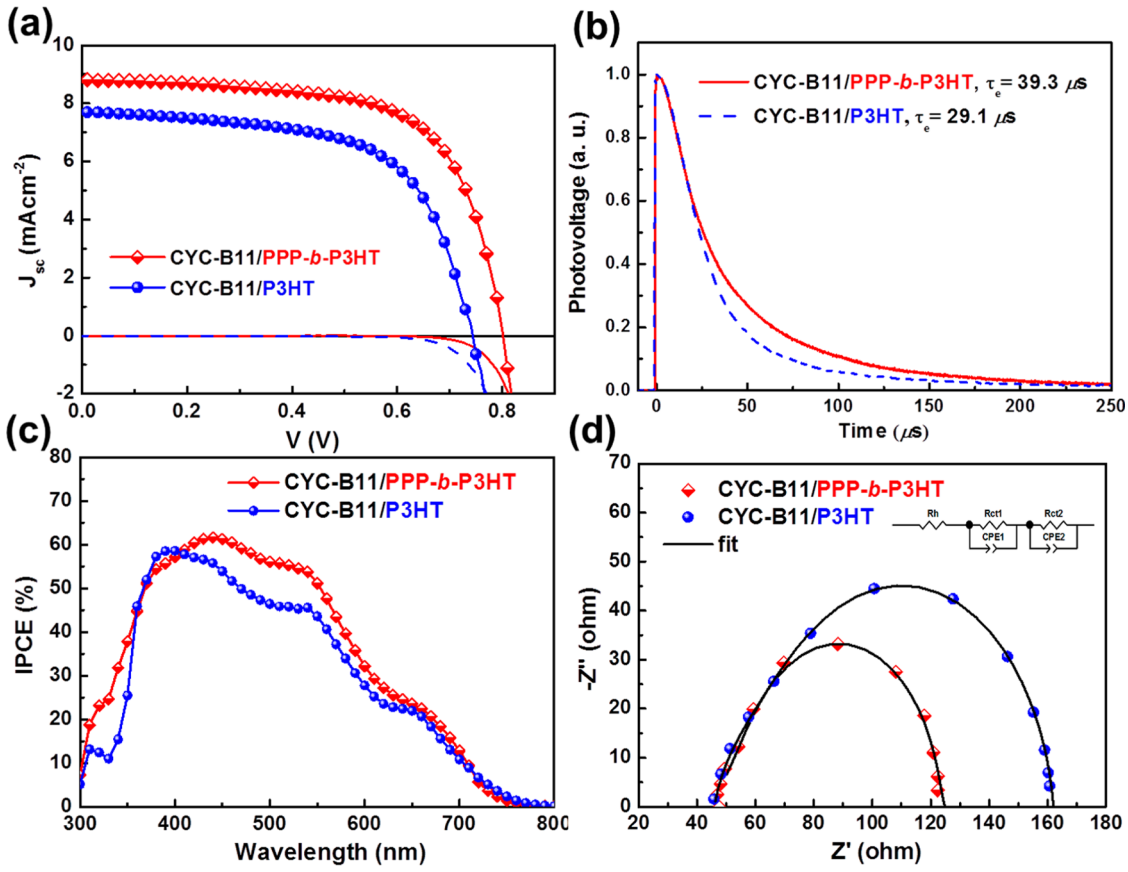

Figure 4. (a) Current density−voltage curves, (b) transient photovoltage curves, (c) incident photo-to-current conversion efficiency spectra, and (d) electrochemical impedance spectra of the ss-DSCs based on CYC-B11/PPP-*b*-P3HT and CYC-B11/P3HT.

TABLE 2. Photovoltaic Characteristics of Solid-State Dye-Sensitized Solar Cells Fabricated from CYC-B11/PPP-*b*-P3HT and CYC-B11/P3HT

device	V_{oc} (V)	J_{sc} (mA/cm^2)	FF (%)	PCE (%)	R_s (Ω cm^2)	R_{sh} (kΩ cm^2)	$R_{ct2,light}$ (Ω)
CYC-B11/PPP-*b*-P3T	0.81	8.81	65.2	4.65	2.31	2.84	58
CYC-B11/P3HT	0.75	7.71	61.1	3.53	2.54	1.87	96

the conduction band of TiO_2 and the HOMO level of HTM, the former device has a higher V_{oc}. To understand this phenomenon, transient photovoltage measurements of the two ss-DSCs were carried out. The average electron lifetime (τ_e) can be readily extracted by fitting the decay curve of the photovoltage transients in Figure 4b with the formula $\exp(-t/\tau_e)$, where t denotes the time that has elapsed after the light pulse is applied. The longer electron lifetime (40 μs) in the PPP-*b*-P3HT cell than that (29 μs) in the analogue P3HT cell suggests a slower charge recombination process at the TiO_2/CYC-B11/HTM interface, leading to a higher V_{oc}. The result can be understood as follows. Inside a ss-DSC, immediately after the electrons on the sensitizer are excited by absorbing incident light, they are rapidly injected into the conduction band of TiO_2, leaving holes on the oxidized sensitizer. These holes can then hop among neighboring dyes[30] and/or be transferred to the HTM. Accordingly, this interfacial charge recombination process essentially proceeds along two possible routes: the back-transfer of the electrons from the TiO_2 conduction band to the cationic dye or to the oxidized HTM. Previous studies have established that the time scale of the transfer of holes from dye cations to solid-state organic molecules ranges from picoseconds to nanoseconds, which is several orders of magnitude shorter than the lifetime of the electrons on TiO_2.[31−33] Therefore, most oxidized dyes that are closely covered with HTM are reasonably assumed to be regenerated before interfacial charges recombine. Consequently, the comparatively short electron lifetime in the P3HT cell may be attributable to incomplete dye coverage with HTM, which leaves stranded holes on dye molecules, and/or the slow movement of holes in HTM, which leads to a small spatial separation between the electrons and the holes.

Figure 4c displays the incident photo-to-current conversion efficiency (IPCE) spectra of the CYC-B11/PPP-*b*-P3HT and CYC-B11/P3HT ss-DSCs. The former cell yields a relatively high IPCE at most wavelengths, and this finding is consistent with the order of magnitude of the J_{sc} values obtained from the $J-V$ curves in

Figure 4a. The small hump in the region of 300–350 nm is caused primarily by the PPP block, whose absorption maximum is at ~340 nm. Although the excitons generated from the photoexcitation of HTM may also contribute to the photocurrent for the ss-DSCs studied herein, the PPP-*b*-P3HT and P3HT have similar UV–vis absorption spectra, as shown in Figure S3b, and the presence of PPP segments inevitably lowers the ability of the copolymer to absorb light in the wavelength range of 400–600 nm to less than that of the P3HT homopolymer at the same mass loading. Therefore, the difference in light-harvesting between the two HTMs is not the main cause of the elevated J_{sc} and the relative high IPCE observed for the CYC-B11/PPP-*b*-P3HT device. Additionally, both cells use the same Ru complex, CYC-B11, as a sensitizer, and both are fabricated from the same TiO_2 paste. These facts imply that replacing P3HT with PPP-*b*-P3HT as HTM may accelerate the generation of excitons in dye molecules.

Electrochemical impedance spectroscopy is a powerful tool for characterizing charge transfer and recombination kinetics in DSCs.[34–37] To gain insight into the interfacial resistance of the two DSCs, EIS measurements were carried out at open-circuit condition and under AM 1.5G illumination with an intensity of 100 mW/cm^2. The Nyquist plots of the two ss-DSCs are shown in Figure 4d, in which the symbols represent the experimental data, while the solid lines represent the fitting obtained by applying the equivalent circuit model shown in the inset of Figure 4d. The resistance values ($R_{ct2,light}$) of the ss-DSCs can then be obtained from the diameter of the fitted semicircles. As shown in Table 2, the CYC-B11/PPP-*b*-P3HT device exhibits a smaller value of $R_{ct2,light}$ (58 Ω) than that (96 Ω) of the CYC-B11/P3HT device, suggesting a relative higher electron density in the conduction band of TiO_2 in the former cell. This result is consistent with the fact that both V_{oc} and J_{sc} of the copolymer device are better than those of the P3HT device. Additionally, we performed the EIS experiments in the dark under various forward biases, in which electrons and holes are injected into the conduction band of TiO_2 and the HOMO of HTM, respectively. The semicircle measured in the frequency range of 1–1000 Hz corresponds mainly to the recombination resistance that is established by the loss of electrons from the conduction band of TiO_2.[38] Figure 5 plots the resistances ($R_{ct2,dark}$) determined from the mid-frequency semicircle as functions of the applied voltage. As in papers published elsewhere,[39] $R_{ct2,dark}$ decreases as the bias voltage increases for both DSCs. Interestingly, the recombination resistance of the PPP-*b*-P3HT cell considerably exceeds that of the P3HT cell, implying that the presence of PPP block effectively reduces the recombination loss of charge carriers at the TiO_2/dye/HTM interface.

Knowledge of the surface free energy of the two components of a block copolymer is essential to understanding the orientation and self-assembly behavior of those macromolecules on a substrate. Herein, the surface free energy and its polar and dispersion components were calculated from the contact angles of water and glycerol on the studied surface using Wu's model, and the results are listed in Table S2. As expected, the bare TiO_2 surface has a high surface energy of ~71 mN/m, which drops significantly to ~12 mN/m after staining with CYC-B11 and then bounces to ~37 mN/m upon subsequent treatments with 4-*tert*-butylpyridine (*t*BP) and bis(trifluoromethane)sulfonimide lithium salt (Li-TFSI). The surface energy of P3HT is determined to be 20.1 mN/m, which is very close to the value reported in the literature[40] and apparently higher than that (17.9 mN/m) of the PPP. The relatively low surface energy of PPP may prevent itself from segregating toward the CYC-B11 surface and therefore provide additional driving force for aligning the P3HT block with the CYC-B11 surface instead, leading to an intimate contact between the P3HT block and the dye-coated surface as a result of better match in their surface energies. Furthermore, the structural similarity between the P3HT and the CYC-B11 sensitizer, which bears two bithiophene end moieties, may also facilitate the motion of the P3HT chains to the dye side. Complete and intimate coverage of the dyed TiO_2 with the HTM, assisted by the two aforementioned driving forces, can synergistically increase the efficiencies of the regeneration of the dye and the transfer of the photoexcited electrons created in P3HT to the TiO_2 anode, increasing both the photocurrent of the solar device and the lifetime of electrons on TiO_2 and reducing the resistance of transferring charges within the TiO_2/dye/HTM.

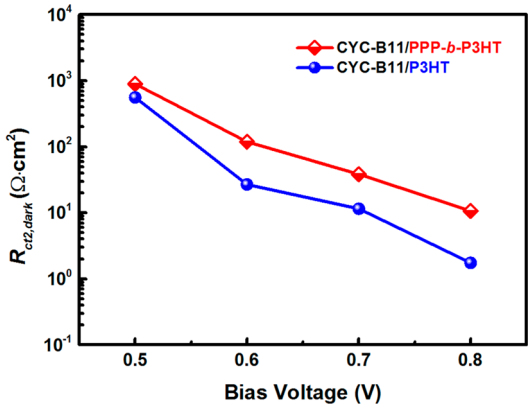

Figure 5. Resistances ($R_{ct2,dark}$) determined from CYC-B11/PPP-*b*-P3HT and CYC-B11/P3HT DSCs in the dark as a function of the applied voltage.

CONCLUSION

In conclusion, ss-DSCs have been fabricated using PPP-*b*-P3HT copolymer as HTM and co-sensitizer. Incorporating a short PPP block into the chain end of P3HT not only enhances the molecular packing of the P3HT segments to form interpenetrated and

long-range-ordered fiber-like crystals but also facilitates the P3HT chains to fully and tightly wrap the CYC-B11 sensitizer upon spin-drying of the solution of such block copolymer on top of the dyed mesoporous TiO_2 layer. The former boosts the hole mobility, thus reducing the rate of carrier recombination and the series resistance of the photovoltaic cell; the latter suppresses the recombination losses occurring at the TiO_2/dye/HTM interface. Consequently, the CYC-B11/PPP-*b*-P3HT cell exhibits a high PCE of 4.65%, that is, approximately 30% higher than that of the analogue cell with P3HT homopolymer as HTM. The present findings demonstrate that conjugated block copolymers are highly promising for use as HTMs, thus opening up a new avenue for the design of novel hole conductors to develop high-performance ss-DSCs.

EXPERIMENTAL SECTION

Materials. TiO_2 paste (Ti Nanoxide HT/SP) was purchased from Salornix. Titanium(IV) chloride ($TiCl_4$, 99.9%), bis(trifluoromethane), Li-TFSI (99.95%), and acetylacetone (99%) were obtained from Acros. Poly(3,4-ethylenedioxythiophene):poly(styrenesulfonate) (PEDOT:PSS, Bytron P AI4083) was purchased from HC Stark and filtered through a 0.25 μm PVDF syringe filter before using. The ruthenium dye, CYC-B11, was synthesized and purified according to the procedure published elsewhere.[41] P3HT was prepared using the Grignard metathesis approach, providing regiocontrol in each coupling step in the polymeric reaction.[42] For the preparation of PPP-*b*-P3HT, the PPP block was synthesized by the polymerization of 1,4-dibromo-2,5-dihexyloxybenzene, followed by the addition of activated 2,5-dibromo-3-hexylthiophene monomer, giving the block copolymer sample.[43]

Device Fabrication. The fluorine-doped SnO_2 (FTO) (Pilkington, 15 Ω/square) substrates were sequentially cleaned with detergent, deionized water, acetone, and isopropyl alcohol in an ultrasonic bath and then dried under N_2 flow. A precursor solution prepared by mixing titanium isopropoxide (0.284 g) with acetylacetone (0.203 g) in ethanol (5.0 mL) was deposited on a cleaned FTO glass, which was preheated to 450 °C, by the spray pyrolysis method using N_2 as carrying gas at a flow rate of 400 mL/min. The film was then calcined at 450 °C for 30 min under air, producing a dense TiO_2 layer with a thickness of around 60 nm. This is followed by the spin-coating of a TiO_2 paste (Ti Nanoxide HT/SP, from Solarnix) to yield a mesoporous TiO_2 film whose thickness was adjusted by varying the spin speed. After being calcined at 450 °C for 30 min and cooled to room temperature, the thus-prepared TiO_2 bilayer was soaked in a $TiCl_4$ aqueous solution (0.05 M) for 30 min at 70 °C, rinsed with deionized water repeatly, annealed in air at 450 °C for 30 min, then cooled to 80 °C, immersed into a ruthenium dye (CYC-B11) solution (0.3 mM, 1:1 acetonitrile/*tert*-butanol) overnight, and last rinsed with acetonitrile three times. Afterward, this dyed TiO_2 film was spin-coated with a mixed solution of Li-TFSI (0.04 M) and *t*BP (0.05 M) in acetonitrile (1000 rpm for 50 s) and dried in N_2 flow, followed by the deposition of a thin layer of the P3HT or the PPP-*b*-P3HT from their chlorobenzene solution with a concentration of 15.0 mg/mL by spin-coating (1000 rpm for 30 s). Finally, the sample was covered with a layer of Ag (100 nm) by thermal evaporation under a vacuum of 10^{-6} Torr in an Edwards Auto 306 vacuum evaporation system through a shadow mask to yield a ss-DSC with an active area of 7 mm^2. The devices used for the SCLC analysis were prepared by depositing a thin film of PEDOT:PSS (40 nm) on top of a precleaned indium-tin-oxide (ITO) glass *via* spin-coating. After being dried at 140 °C for 10 min in air and then transferred to a nitrogen-filled glovebox, the sample was spin-coated with a layer of the PPP-*b*-P3HT or the P3HT (~100 nm). Subsequently, a gold electrode (70 nm) was formed on top of the studied polymer by thermal evaporation to complete the device fabrication.

Characterization. ^{1}H NMR spectra were recorded on a 400 MHz Bruker Avance spectrometer. Gel permeation chromatography was carried out on a Waters 2695 system equipped with two Waters styragel columns (HR3 and HR4E), a refractive index detector (Waters 2414), and a photodiode array absorbance detector (Waters 2996) using tetrahydrofuran (THF) as eluent and a set of polystyrene standards (Pressure Chemicals) as standard to construct the calibration curve. Samples for WAXS measurements were prepared by spin-coating the corresponding polymer solution (1.5 wt %) on a 1 mm thick silicon wafer. The WAXS experiments were performed with an irradiation wavelength of 1.03051 Å at the 13A1 endstation of the National Synchrotron Radiation Research Center (NSRRC) of Taiwan. Samples for TEM measurements were prepared by spin-coating a polymer solution (1.5 wt %) on a 1 mm thick silicon wafer which was precoated with a PEDOT:PSS layer, followed by floating the polymer film off the silicon substrate in water and picking it up onto a copper grid. Bright-field images were captured on a JEOL 1230EX TEM operating at 120 kV with a Gaten Dual Vision CCD camera. UV−vis absorption spectra were taken on a Jasco V-670 UV/vis spectrophotometer. CV measurements were performed in an anhydrous dimethylformamide (DMF) solution containing 0.1 M *tetra-n*-butylammonium hexafluorophosphate under N_2 atmosphere using a CHI 660 electrochemical analyzer with a glassy carbon, a Pt plate, and a saturated aqueous Ag/Ag^+ electrode as the working, counter, and reference electrodes, respectively, at a scan rate of 30 mV/s. The reference electrode was calibrated by running the CV of ferrocene without the analyte. The *J*−*V* characteristics of photovoltaic devices were evaluated with a Keithley 2400 source meter under AM 1.5G solar irradiation obtained from a 300 W Oriel solar simulator, at an intensity of 100 mW/cm^2, which was calibrated by a mono-Si reference cell with a KG5 filter. The SCLC measurements were carried out using a Keithley 2400 source meter under dark condition. The IPCE spectra were recorded under illumination by a xenon lamp and a monochromator (TRIAX 180, JOBIN YVON), and the light intensity was calibrated by using an OPHIR 2A-SH thermopile detector. Transient photovoltage measurements were conducted under AM 1.5G illumination at 80 mW/cm^2 with a pulsed laser excitation by a frequency-double Q-switched Nd:YAG laser (model Quanta-Ray GCR-3-10, Spectra-Physics laser) with a 2 Hz repetition rate at 532 nm, and a 7 ns pulse width at half-height. Electrochemical impedance spectroscopy was obtained under AM 1.5G illumination at 1 sun and in the dark on a PGSTAT 30 potentiostat/galvanostat (Autolab, Eco-Chemie, The Netherlands) equipped with an FRA2 module.

Conflict of Interest: The authors declare no competing financial interest.

Acknowledgment. The authors thank National Taiwan University, National Central University, Academia Sinica, and the National Science Council of the Republic of China (NSC 100-3113-E-008-003; NSC 99-2113-M-002-001-MY3) for financially supporting this research.

Supporting Information Available: Synthetic route, GPC, ^{1}H NMR spectrum of PPP-*b*-P3HT, UV−vis and CV analysis, surface energy measurements, and photovoltaic parameters of photovoltaic devices are included. This material is available free of charge *via* the Internet at http://pubs.acs.org.

REFERENCES AND NOTES

1. Stathatos, E. Dye Sensitized Solar Cells as an Alternative Approach to the Conventional Potovoltaic Technology Based on Silicon: Recent Development in the Field and Large Scale Applications. In *Solar Cells: Dye-Sensitized Devices*; Kosyachenko, L. A., Eds.; InTech: Athens, Greece, 2011; pp 471−492.

2. Hagfeldt, A.; Boschloo, G.; Sun, L.; Kloo, L.; Pettersson, H. Dye-Sensitized Solar Cells. *Chem. Rev.* **2010**, *110*, 6595–6663.
3. Yella, A.; Lee, H.-W.; Tsao, H. N.; Yi, C.; Chandiran, A. K.; Nazeeruddin, M. K.; Diau, E. W.-G.; Yeh, C.-Y.; Zakeeruddin, S. M.; Grätzel, M. Porphyrin-Sensitized Solar Cells with Cobalt(II/III)-Based Redox Electrolyte Exceed 12% Efficiency. *Science* **2011**, *334*, 629–633.
4. Schmidt-Mende, L.; Bach, U.; Humphry-Baker, R.; Horiuchi, T.; Miura, H.; Ito, S.; Uchida, S.; Grätzel, M. Organic Dye for Highky Efficient Solid-State Dye-Sensitized Solar Cells. *Adv. Mater.* **2005**, *17*, 813–815.
5. Wang, P.; Zakeeruddin, S. M.; Moser, J. E.; Nazeeruddin, M. K.; Sekiguchi, T.; Grätzel, M. A Stable Quasi-Solid-State Dye-Sensitized Solar Cell with an Amphiphilic Ruthenium Sensitizer and Polymer Gel Electrolyte. *Nat. Mater.* **2003**, *2*, 402–407.
6. Bach, U. Solid-State Dye-Sensitized Solar Cells: An Alternative Route toward Low-Cost Photovoltaic Device. In *Encyclopedia of Electrochemistry*; Wiley-VCH: Weinheim, Germany, 2007; pp 475−491.
7. Yum, J.-H.; Chen, P.; Grätzel, M.; Nazeeruddin, M. K. Recent Developments in Solid-State Dye-Sensitized Solar Cells. *ChemSusChem* **2008**, *1*, 699–707.
8. Leijtens, T.; Ding, I.-K.; Giovenzana, T. J.; Blocking, T.; McGehee, M. D.; Sellinger, A. Hole Transport Materials with Low Glass Transition Temperatures and High Solubility for Application in Solid-State Dye-Sensitized Solar Cells. *ACS Nano* **2012**, *6*, 1455–1462.
9. Hodes, G.; Cahen, D. All-Solid-State, Semiconductor-Sensitized Nanoporous Solar Cells. *Acc. Chem. Res.* **2012**, *45*, 705–713.
10. Chung, I.; Lee, B.; He, J.; Chang, R. P. H.; Kanatzidis, M. G. All-Solid-State Dye-Sensitized Solar Cells with High Efficiency. *Nature* **2012**, *485*, 486–489.
11. Bach, U.; Cloedt, K. D.; Spreitizer, H.; Grätzel, M. Characterization of Hole Transport in a New Class of Spiro-Linked Oligotriphenylamine Compounds. *Adv. Mater.* **2000**, *12*, 1060–1063.
12. Zhang, W.; Cheng, Y.; Yin, X.; Liu, B. Solid-State Dye-Sensitized Solar Cells with Conjugated Polymers as Hole-Transporting Materials. *Macromol. Chem. Phys.* **2011**, *212*, 15–23.
13. Günes, S.; Neugebauer, H.; Sariciftci, N. S. Conjugated Polymer-Based Organic Solar Cells. *Chem. Rev.* **2007**, *107*, 1324–1338.
14. Grancini, G.; Kumar, R. S. S.; Abrusci, A.; Yip, H.-L.; Li, C.-Z.; Jen, A.-K. Y.; Lanzani, G.; Snaith, H. J. Boosting Infrared Light Harvesting by Molecular Functionalization of Metal Oxide/Polymer Interfaces in Efficient Hybrid Solar Cells. *Adv. Funct. Mater.* **2012**, *22*, 2160–2166.
15. Jiang, K.-J.; Manseki, K.; Yu, Y.-H.; Masaki, N.; Suzuki, K.; Song, Y.-L.; Yanagida, S. Photovoltaics Based on Hybridization of Effective Dye-Sensitized Titanium Oxide and Hole-Conductive Polymer P3HT. *Adv. Funct. Mater.* **2009**, *19*, 2481–2485.
16. Moon, S.-J.; Baranoff, E.; Zakeeruddin, S. M.; Yeh, C.-Y.; Diau, E. W.-G.; Grätzel, M.; Sivula, K. Enhanced Light Harvesting in Mesoporous TiO_2/P3HT Hybrid Solar Cells Using a Porphyrin Dye. *Chem. Commun.* **2011**, *47*, 8244–8246.
17. Snaith, H. J.; Grätzel, M. Electron and Hole Transport through Mesoporous TiO_2 Infiltrated with Spiro-MeOTAD. *Adv. Mater.* **2007**, *19*, 3643–3647.
18. Melas-Kyriazi, J.; Ding, I.-K.; Marchioro, A.; Punzi, A.; Hardin, B. E.; Burkhard, G. F.; Tétreault, N.; Grätzel, M.; Moser, J.-E.; McGehee, M. D. The Effect of Hole Transport Material Pore Filling on Photovoltaic Performance in Solid-State Dye-Sensitized Solar Cells. *Adv. Energy Mater.* **2011**, *1*, 407–414.
19. Snaith, H. J.; Humphry-Baker, R.; Chen, P.; Cesar, I.; Zakeeruddin, S. M.; Grätzel, M. Charge Collection and Pore Filling in Solid-State Dye-Sensitized Solar Cells. *Nanotechnology* **2008**, *19*, 424003.
20. Snaith, H. J.; Schmidt-Mende, L. Advances in Liquid-Electrolyte and Solid-State Dye-Sensitized Solar Cells. *Adv. Mater.* **2007**, *19*, 3187–3200.
21. Chen, W.-C.; Chen, C.-Y.; Wu, C.-G.; Ho, K.-C.; Wang, L. Effect of Structural Compatibility of Dye and Hole Transport Material on Performance of Solid-State Dye-Sensitized Solar Cells. *J. Power Sources* **2012**, *214*, 113–118.
22. Hamley, I. W. *The Physics of Block Copolymers*; Oxford University Press: New York, 1998.
23. Bates, F. S.; Fredrickson, G. H. Block Copolymers—Designer Soft Materials. *Phys. Today* **1999**, *52*, 32–38.
24. Yu, X.; Yang, H.; Wu, S.; Geng, Y.; Han, Y. Microphase Separation and Crystallization of All-Conjugated Phenylene−Thiophene Diblock Copolymers. *Macromolecules* **2012**, *45*, 266–274.
25. Kline, R. J.; McGehee, M. D.; Kadnikova, E. N.; Liu, J.; Fréchet, J. M. J.; Toney, M. F. Dependence of Regioregular Poly(3-hexylthiophene) Film Morphology and Field-Effect Mobility on Molecular Weight. *Macromolecules* **2005**, *38*, 3312–3319.
26. Kline, R. J.; McGehee, M. D.; Kadnikova, E. N.; Liu, J.; Fréchet, J. M. J. Controlling the Field-Effect Mobility of Regioregular Polythiophene by Changing the Molecular Weight. *Adv. Mater.* **2003**, *15*, 1519–1522.
27. Chang, Y.-M.; Su, W.-F.; Wang, L. Influence of Photo-induced Degradation on the Optoelectronic Properties of Regioregular Poly(3-hexylthiophene). *Sol. Energy Mater. Sol. Cells* **2008**, *92*, 761–765.
28. Goh, C.; Kline, R. J.; McGehee, M. D.; Kadnikova, E. N.; Fréchet, J. M. J. Molecular-Weight-Dependent Mobilities in Regioregular Poly(3-hexyl-thiophene) Diodes. *Appl. Phys. Lett.* **2005**, *86*, 122110.
29. Zhu, R.; Jiang, C.-Y.; Liu, B.; Ramakrishna, S. Highly Efficient Nanoporous TiO_2-Polythiophene Hybrid Solar Cells Based on Interfacial Modification Using a Metal-Free Organic Dye. *Adv. Mater.* **2008**, *20*, 1–7.
30. Abrusci, A.; Ding, I.-K.; Al-Hamshimi, M.; Segal-Peretz, T.; McGehee, M. D.; Heeney, M.; Frey, G. L.; Snaith, H. J. Facile Infiltration of Semiconducting Polymer into Mesoporous Electrodes for Hybrid Solar Cells. *Energy Environ. Sci.* **2011**, *4*, 3051–3058.
31. Grätzel, M. Dye-Sensitized Solid-State Heterojunction Solar Cells. *MRS Bull.* **2005**, *30*, 23–27.
32. Bach, U.; Tachibana, Y.; Moser, J.-E.; Haque, S. A.; Durrent, J. R.; Grätzel, M.; King, D. R. Charge Separation in Solid-State Dye-Sensitized Heterojunction Solar Cells. *J. Am. Chem. Soc.* **1999**, *121*, 7445–7446.
33. Krüger, J.; Plass, R.; Cevey, L.; Piccirelli, M.; Grätzel, M. High Efficiency Solid-State Photovoltaic Device due to Inhibition of Interface Charge Recombination. *Appl. Phys. Lett.* **2001**, *79*, 2085–2087.
34. Choi, H.; Kim, S.; Kang, S. O.; Ko, J.; Kang, M.-S.; Clifford, J. N.; Forneli, A.; Palomares, E.; Nazeeruddin, M. K.; Grätzel, M. Stepwise Cosensitization of Nanocrystalline TiO_2 Films Utilizing Al_2O_3 Layers in Dye-Sensitized Solar Cells. *Angew. Chem., Int. Ed.* **2008**, *47*, 8259–8263.
35. Koh, J. K.; Kim, J.; Kim, B.; Kim, J. H.; Kim, E. Highly Efficient, Iodine-Free Dye-Sensitized Solar Cells with Solid-State Synthesis of Conducting Polymers. *Adv. Mater.* **2011**, *23*, 1641–1646.
36. Caballero, R.; Barea, E. M.; Fabregat-Santiago, F.; de la Cruz, P.; Marquez, L.; Langa, F.; Bisquert, J. Injection and Recombination in Dye-Sensitized Solar Cells with a Broadband Absorbance. *J. Phys. Chem. C* **2008**, *112*, 18623–18627.
37. Xu, C.; Wu, J.; Desai, U. V.; Gao, D. High-Efficiency Solid-State Dye-Sensitized Solar Cells Based on TiO_2-Coated ZnO Nanowire Arrays. *Nano Lett.* **2012**, *12*, 2420–2424.
38. Chen, C.-Y.; Pootrakulchote, N.; Wu, S.-J.; Wang, M.; Li, J.-Y.; Tsai, J.-H.; Wu, C.-G.; Zakeeruddin, S. M.; Grätzel, M. New Ruthenium Sensitizer with Carbazole Antennas for Efficient and Stable Thin-Film Dye-Sensitized Solar Cells. *J. Phys. Chem. C* **2009**, *113*, 20752–20757.
39. Sauvage, F.; Decoppet, J.-D.; Zhang, M.; Zakeeruddin, S. M.; Comte, P.; Nazeeruddin, M.; Wang, P.; Grätzel, M. Effect of Sensitizer Adsorption Temperature on the Performance of Dye-Sensitized Solar Cells. *J. Am. Chem. Soc.* **2011**, *133*, 9304–9310.
40. Bulliard, X.; Ihn, S.-G.; Yun, S.; Kim, Y.; Choi, D.; Choi, J.-Y.; Kim, M.; Sim, M.; Park, J.-H.; Choi, W.; *et al.* Enhanced Performance in Polymer Solar Cells by Surface Energy Control. *Adv. Funct. Mater.* **2010**, *20*, 4381–4387.

41. Chen, C.-Y.; Wang, M.; Li, J.-Y.; Pootrakulchote, N.; Alibabaei, L.; Ngoc-le, C.-H.; Decoppet, J.-D.; Tsai, J.-H.; Grätzel, C.; Wu, C.-G.; *et al.* Highly Efficient Light-Harvesting Ruthenium Sensitizer for Thin-Film Dye-Sensitized Solar Cells. *ACS Nano* **2009**, *3*, 3103–3109.
42. Chen, T.-A.; Rieke, R. D. The First Regioregular Head-to-Tail Poly(3-hexylthiophene-2,5-diyl) and a Regiorandom Isopolymer: Ni *vs.* Pd Catalysis of 2(5)-Bromo-5(2)-(bromozincio)-3-hexylthiophene Polymerization. *J. Am. Chem. Soc.* **1992**, *114*, 10087–10088.
43. Miyakoshi, R.; Yokoyama, A.; Yokozawa, T. Importance of the Order of Successive Catalyst-Transfer Condensation Polymerization in the Synthesis of Block Copolymers of Polythiophene and Poly(*p*-phenylene). *Chem. Lett.* **2008**, *37*, 1022–1023.